Wireless Location Tracking Algorithms for Environments with Insufficient Signal Sources

Po-Hsuan Tseng, *Student Member*, *IEEE*, Kai-Ten Feng, *Member*, *IEEE*, Yu-Chiun Lin, and Chao-Lin Chen

Abstract—Location estimation and tracking for the mobile devices have attracted a significant amount of attention in recent years. The network-based location estimation schemes have been widely adopted based on the radio signals between the mobile device and the base stations. The location estimators associated with the Kalman filtering techniques are exploited to both acquire location estimation and trajectory tracking for the mobile devices. However, most of the existing schemes become inapplicable for location tracking due to the deficiency of signal sources. In this paper, two predictive location tracking algorithms are proposed to alleviate this problem. The Predictive Location Tracking (PLT) scheme utilizes the predictive information obtained from the Kalman filter in order to provide the additional signal inputs for the location estimator. Furthermore, the Geometric-assisted PLT (GPLT) scheme incorporates the Geometric Dilution of Precision (GDOP) information into the algorithm design. Persistent accuracy for location tracking can be achieved by adopting the proposed GPLT scheme, especially with inadequate signal sources. Numerical results demonstrate that the GPLT algorithm can achieve better precision in comparison with other network-based location tracking schemes.

Index Terms—Wireless location estimation, Kalman filter, geometric dilution of precision (GDOP), two-step least-square estimators.

1 Introduction

Wireless location technologies, which are designated to estimate the position of a Mobile Station (MS), have drawn a lot of attention over the past few decades. The Quality-of-Service (QoS) of the positioning accuracy has been announced after the issue of the emergency 911 (E-911) subscriber safety service [1]. With the assistance of the information derived from the positioning system, the required performance and objectives for the targeting MS can be achieved with augmented robustness. In recent years, there are increasing demands for commercial applications to adopt the location information within their system design, such as the navigation systems, the location-based billing, the health care systems, the Wireless Sensor Networks (WSNs) [2], [3], [4], and the Intelligent Transportation Systems (ITSs) [5], [6]. With the emergent interests in the Location-Based Services (LBSs), the location estimation algorithms with enhanced precision become necessary for the applications under different circumstances.

A variety of wireless location techniques have been investigated [7], [8], [9], [10]. The network-based location estimation schemes have been widely proposed and employed in the wireless communication system. These schemes locate the position of an MS based on the measured radio signals from its neighborhood Base Stations (BSs). The representative algorithms for the network-based location estimation techniques are the Time-of-Arrival (TOA), the Time Difference-of-Arrival (TDOA), and the Angle-of-Arrival (AOA). The TOA scheme measures the arrival time of the radio signals coming from different wireless BSs; while the TDOA scheme measures the time difference between the radio signals. The AOA technique is conducted within the BS by observing the arriving angle of the signals coming from the MS.

It is recognized that the equations associated with the network-based location estimation schemes are inherently nonlinear. The uncertainties induced by the measurement noises make it more difficult to acquire the estimated MS position with tolerable precision. The Taylor Series Expansion (TSE) method was utilized in [11] to acquire the location estimation of the MS from the TOA measurements. The method requires iterative processes to obtain the location estimate from a linearized system. The major drawback of the TSE scheme is that it may suffer from the convergence problem due to an incorrect initial guess of the MS's position. The two-step Least-Square (LS) method was adopted to solve the location estimation problem from the TOA [12], the TDOA [13], and the TDOA/AOA measurements [14]. It is an approximate realization of the Maximum Likelihood (ML) estimator and does not require iterative processes. The two-step LS scheme is advantageous in its computational efficiency with adequate accuracy for location estimation. Instead of utilizing the Circular Line of Position (CLOP) methods (e.g., the TSE and the two-step LS schemes), the Linear Line of Position (LLOP) approach is presented as a different interpretation for the cell geometry from the TOA measurements. Since the pairwise intersections of N TOA measurements will establish $(N-1)$ independent linear lines, the LS method can, therefore, be applied to estimate the position of the MS. The detail algorithm of the LLOP

- *P.-H. Tseng and K.-T. Feng are with the Department of Communication Engineering, National Chiao Tung University, Hsinchu, Taiwan, R.O.C. E-mail: walker.cm90g@nctu.edu.tw, ktfeng@mail.nctu.edu.tw.*
- *Y.-C. Lin is with Pegatron Corporation, Taipei, Taiwan, R.O.C. E-mail: tino.cm94g@nctu.edu.tw.*
- *C.-L. Chen is with TrendChip Technologies Corporation, Hsinchu, Taiwan, R.O.C. E-mail: sart.cm92g@nctu.edu.tw.*

Manuscript received 18 Aug. 2007; revised 11 June 2008; accepted 10 Apr. 2009; published online 21 Apr. 2009.
For information on obtaining reprints of this article, please send e-mail to: tmc@computer.org, and reference IEEECS Log Number TMC-2007-08-0248. Digital Object Identifier no. 10.1109/TMC.2009.75.

approach can be obtained by using the TOA measurements as in [15], and the hybrid TOA/AOA measurements in [16].

In addition to the estimation of an MS's position, trajectory tracking of a moving MS has been studied [17], [18], [19], [20], [21], [22], [23], [24]. The Extended Kalman Filter (EKF) scheme [17], [18], [19] is considered the well-adopted method for location tracking. The EKF algorithm estimates the MS's position, speed, and acceleration via the linearization of measurement inputs. The technique by combining the Kalman filter with the Weighted Least-Square (WLS) method is exploited in [20]. The Kalman Tracking (KT) scheme [21], [22] distinguishes the linear part from the originally nonlinear equations for location estimation. The linear aspect is exploited within the Kalman filtering formulation; while the nonlinear term is served as an external measurement input to the Kalman filter. The technique utilized in [23] adopted the Kalman filters for both preprocessing and postprocessing in order to both mitigate the Nonline-of-Sight (NLOS) noises and track the MS's trajectory. The Cascade Location Tracking (CLT) scheme as proposed in [24] utilizes the two-step LS method for initial location estimation of the MS. The Kalman filtering technique is employed to smooth out and trace the position of the MS based on its previously estimated data.

The Geometric Dilution of Precision (GDOP) [25], [26] and the Cramér-Rao Lower Bound (CRLB) [27] are the well-adopted metrics for justifying the accuracy of location estimation based on the geometric layouts between the MS and its associated BSs. It has been indicated in [28] that the environments with ill-conditioned layouts will result in relatively larger GDOP and CRLB values. In general, the ill-conditioned situations can be classified into two categories: 1) insufficient number of available neighborhood BSs around the MS and 2) the occurrence of collinearity or coplanarity between the BSs and the MS. It is noticed that the problem caused by case 2 can be resolved with well-planned locations of the BSs. Nevertheless, the scenarios with insufficient signal sources (i.e., case 1) can happen in real circumstances, e.g., under rural environments or city valley with blocking buildings. It will be beneficial to provide consistent accuracy for location tracking under various environments. However, the wireless location tracking problem with deficient signal sources has not been extensively addressed in previous studies. In the cellular-based networks, three BSs are required in order to provide three signal sources for the TOA-based location estimation. The scheme as proposed in [29] considers the location tracking problem under the circumstances with short periods of signal deficiency, i.e., occasionally with only two signal sources available. The linear predictive information obtained from the Kalman filter is injected into its original LS scheme while one of the BSs is not observable. However, this algorithm is regarded as a preliminary design for signal-deficient scenarios, which does not consider the cases while only one BS is available for location estimation. Insufficient accuracy for location estimation and tracking of the MS is, therefore, perceived.

In this paper, a Predictive Location Tracking (PLT) algorithm is proposed to improve the problem with insufficient measurement inputs, i.e., with only two BSs or a single BS available to be exploited. The predictive information obtained from the Kalman filter is adopted as the virtual signal source, which is incorporated into the two-step LS method for location estimation and tracking. It is also noted that the preliminary design of the PLT scheme was first presented in our previous work in [30]. A more comprehensive design and performance comparison with other schemes will be conducted in this paper. Moreover, a Geometric-assisted Predictive Location Tracking (GPLT) scheme is proposed by adopting the GDOP concept into its formulation in order to further enhance the performance of the original PLT algorithm. The position of the virtual signal source is relocated for the purpose of achieving the minimum GDOP value with respect to the MS's position. Consistent precision for location tracking of an MS is observed by exploiting the GPLT algorithm. Comparing with the existing techniques, the simulation results show that the proposed GPLT scheme can acquire higher accuracy for location estimation and tracking even under the situations with inadequate signal sources.

The remainder of this paper is organized as follows: Section 2 briefly describes the modeling of the signal sources, the two-step LS estimator, and the GDOP metric. The concepts and motivations of the proposed PLT and GPLT schemes are explained in Section 3. Section 4 presents the PLT algorithm with two different scenarios; while the formulation of the GPLT scheme is exploited in Section 5. Section 6 illustrates the performance evaluation of the proposed PLT and the GPLT schemes in comparison with the existing location tracking techniques. Section 7 draws the conclusions.

2 Preliminaries

2.1 Mathematical Modeling

In order to facilitate the design of the proposed PLT and the GPLT algorithms, the signal model for the TOA measurements is utilized. The set $\boldsymbol{r}_k$ contains all the available measured relative distance at the kth time step, i.e., $\boldsymbol{r}_k = \{r_{1,k}, \ldots, r_{i,k}, \ldots, r_{N_k,k}\}$, where N_k denotes the number of available BSs at the time step k. The measured relative distance ($r_{i,k}$) between the MS and the ith BS (obtained at the kth time step) can be represented as

$$r_{i,k} = c \cdot t_{i,k} = \zeta_{i,k} + n_{i,k} + e_{i,k} \qquad i = 1, 2, \ldots, N_k, \tag{1}$$

where $t_{i,k}$ denotes the TOA measurement obtained from the ith BS at the kth time step, and c is the speed of light. $r_{i,k}$ is contaminated with the TOA measurement noise $n_{i,k}$ and the NLOS error $e_{i,k}$. It is noted that the measurement noise $n_{i,k}$ is, in general, considered as zero mean with Gaussian distribution. On the other hand, the NLOS error $e_{i,k}$ is modeled as exponentially distributed for representing the positive bias due to the NLOS effect [31], [32]. The noiseless relative distance $\zeta_{i,k}$ (in (1)) between the MS's true position and the ith BS can be obtained as

$$\zeta_{i,k} = [(x_k - x_{i,k})^2 + (y_k - y_{i,k})^2]^{\frac{1}{2}}, \tag{2}$$

where $\boldsymbol{x}_k = [x_k\ y_k]$ represents the MS's true position and $\boldsymbol{x}_{i,k} = [x_{i,k}\ y_{i,k}]$ is the location of the ith BS for $i = 1$ to N_k.

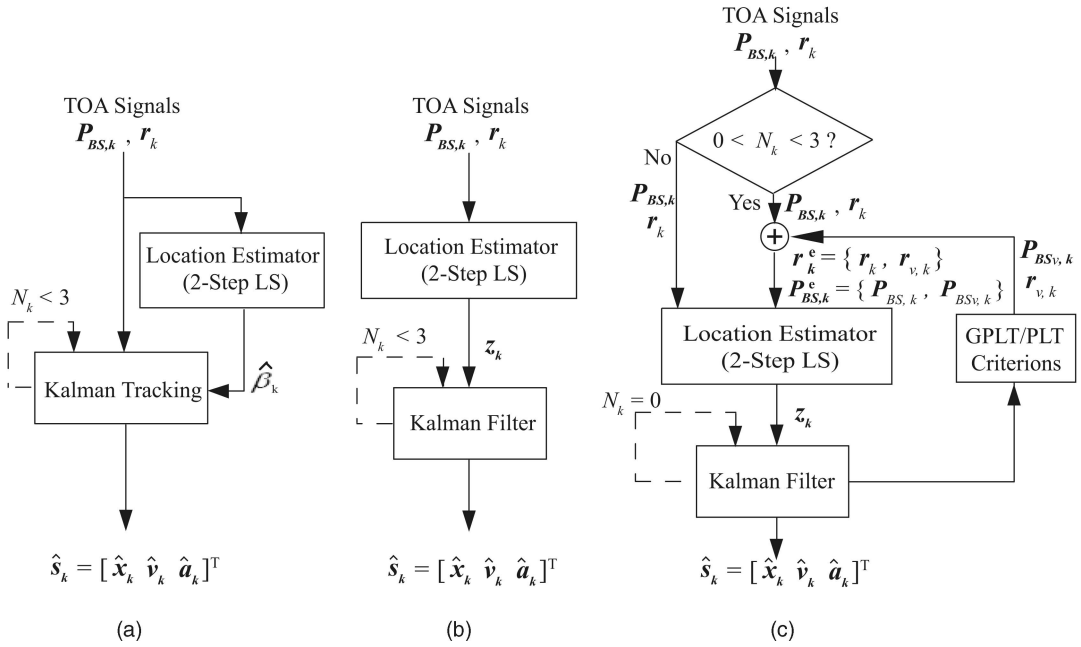

Fig. 1. The architecture diagrams of (a) the Kalman Tracking (KT) scheme; (b) the Cascade Location Tracking (CLT) scheme; and (c) the proposed Predictive Location Tracking (PLT) and Geometric-assisted Predictive Location Tracking (GPLT) schemes.

Therefore, the set of all the available BSs at the kth time step can be obtained as $\boldsymbol{P}_{BS,k} = \{\boldsymbol{x}_{1,k}, \ldots, \boldsymbol{x}_{i,k}, \ldots, \boldsymbol{x}_{N_k,k}\}$.

2.2 Two-Step LS Estimator

The two-step LS scheme [12], [13], [14] is utilized as the baseline location estimator for the proposed predictive location tracking algorithms. It is noticed that three TOA measurements are required for the two-step LS method in order to solve for the location estimation problem. The concept of the two-step LS scheme is to acquire an intermediate location estimate in the first step with the definition of a new variable β_k, which is mathematically related to the MS's position, i.e., $\beta_k = x_k^2 + y_k^2$. At this stage, the variable β_k is assumed to be uncorrelated to the MS's position. This assumption effectively transforms the nonlinear equations for location estimation into a set of linear equations, which can be directly solved by the LS method. Moreover, the elements within the associated covariance matrix are selected based on the standard deviation from the measurements. The variations within the corresponding signal paths are, therefore, considered within the problem formulation.

The second step of the method primarily considers the relationship that the variable β_k is equal to $x_k^2 + y_k^2$, which was originally assumed to be uncorrelated in the first step. An improved location estimation can be obtained after the adjustment from the second step. The detail algorithm of the two-step LS method for location estimation can be found in [12].

2.3 Geometric Dilution of Precision

The GDOP [25] associated with the position error is utilized as an index for observing the location precision of the MS under different geometric locations within the networks, e.g., the cellular or the satellite networks. In general, a larger GDOP value corresponds to a comparably worse geometric layout (established by the MS and its associated BSs), which, consequently, results in augmented errors for location estimation. Considering the MS's location under the two-dimensional coordinate, the GDOP value (G) obtained at the position $\boldsymbol{x}_k$ can be represented as

$$\mathrm{G}_{\boldsymbol{x}_k} = \left\{\mathrm{trace}\left[(\mathbf{H}_{\boldsymbol{x}_k}^T \mathbf{H}_{\boldsymbol{x}_k})^{-1}\right]\right\}^{\frac{1}{2}}, \tag{3}$$

where

$$\mathbf{H}_{\boldsymbol{x}_k} = \begin{bmatrix} \frac{x_k - x_{1,k}}{\zeta_{1,k}} & \frac{y_k - y_{1,k}}{\zeta_{1,k}} \\ \cdots & \cdots \\ \frac{x_k - x_{i,k}}{\zeta_{i,k}} & \frac{y_k - y_{i,k}}{\zeta_{i,k}} \\ \cdots & \cdots \\ \frac{x_k - x_{N_k,k}}{\zeta_{N_k,k}} & \frac{y_k - y_{N_k,k}}{\zeta_{N_k,k}} \end{bmatrix}. \tag{4}$$

It is noted that the elements within the matrix $\mathbf{H}_{\boldsymbol{x}_k}$ can be acquired from (2). It has been shown in [25] that the minimum GDOP value frequently occurs around the center of the network layout, e.g., the minimum GDOP inside a K-side ($K \geq 3$) regular polygon is shown to take place at the center of the layout and the value is obtained as $\mathrm{G} = \frac{2}{\sqrt{K}}$. Moreover, the GDOP and CRLB values are demonstrated to be identical given a Gaussian-distributed noise model [26].

3 Architecture Overview of Proposed PLT and GPLT Algorithms

The objective of the proposed PLT and the GPLT algorithms is to utilize the predictive information acquired from the Kalman filter to serve as the assisted measurement inputs while the environments are deficient with signal sources. Fig. 1 illustrates the system architectures of the KT [21], the CLT [24], and the proposed PLT/GPLT schemes. The TOA signals ($\boldsymbol{r}_k$ as in (1)) associated with the corresponding

location set of the BSs ($\boldsymbol{P}_{BS,k}$) are obtained as the signal inputs to each of the system, which result in the estimated state vector of the MS, i.e., $\hat{\boldsymbol{s}}_k = [\hat{\boldsymbol{x}}_k\ \hat{\boldsymbol{v}}_k\ \hat{\boldsymbol{a}}_k]^T$, where $\hat{\boldsymbol{x}}_k = [\hat{x}_k\ \hat{y}_k]$ represents the MS's estimated position, $\hat{\boldsymbol{v}}_k = [\hat{v}_{x,k}\ \hat{v}_{y,k}]$ is the estimated velocity, and $\hat{\boldsymbol{a}}_k = [\hat{a}_{x,k}\ \hat{a}_{y,k}]$ denotes the estimated acceleration.

Since the equations (i.e., (1) and (2)) associated with the network-based location estimation are intrinsically nonlinear, different mechanisms are considered within the existing algorithms for location tracking. The KT scheme [21] (as shown in Fig. 1a) explores the linear aspect of location estimation within the Kalman filtering formulation; while the nonlinear term (i.e., $\hat{\beta}_k = \hat{x}_k^2 + \hat{y}_k^2$) is treated as an additional measurement input to the Kalman filter. It is stated within the KT scheme that the value of the nonlinear term can be obtained from an external location estimator, e.g., via the two-step LS method. Consequently, the estimation accuracy of the KT algorithm largely depends on the precision of the additional location estimator. On the other hand, the CLT scheme [24] (as illustrated in Fig. 1b) adopts the two-step LS method to acquire the preliminary location estimate of the MS. The Kalman Filter is utilized to smooth out the estimation error by tracing the estimated state vector $\hat{\boldsymbol{s}}_k$ of the MS.

The architecture of the proposed PLT and GPLT schemes is illustrated in Fig. 1c. It is noticed that the GPLT algorithm involves additional transformation via the GDOP calculation compared with the PLT scheme. It can be seen that the PLT/GPLT algorithms will be the same as the CLT scheme while $N_k \geq 3$, i.e., the number of available BSs is greater than or equal to three. However, the effectiveness of the PLT/GPLT schemes is revealed as $1 \leq N_k < 3$, i.e., with deficient measurement inputs. The predictive state information obtained from the Kalman filter is utilized for acquiring the assisted information, which will be fed back into the location estimator. The extended sets for the locations of the BSs (i.e., $\boldsymbol{P}^e_{BS,k} = \{\boldsymbol{P}_{BS,k},\ \boldsymbol{P}_{BS_v,k}\}$) and the measured relative distances (i.e., $\boldsymbol{r}^e_k = \{\boldsymbol{r}_k,\ \boldsymbol{r}_{v,k}\}$) will be utilized as the inputs to the location estimator. The sets of the virtual BS's locations $\boldsymbol{P}_{BS_v,k}$ and the virtual measurements $\boldsymbol{r}_{v,k}$ are defined by the following definitions.

Definition 1 (Virtual Base Stations). *Within the PLT/GPLT formulation, the virtual Base Stations are considered as the designed locations for assisting the location tracking of the MS under the environments with deficient signal sources. The set of virtual BSs $\boldsymbol{P}_{BS_v,k}$ is defined under two different numbers of N_k as*

$$\boldsymbol{P}_{BS_v,k} = \begin{cases} \{\boldsymbol{x}_{v_1,k}\}, & for\ N_k = 2 \\ \{\boldsymbol{x}_{v_1,k},\ \boldsymbol{x}_{v_2,k}\}, & for\ N_k = 1. \end{cases} \tag{5}$$

Definition 2 (Virtual Measurements). *Within the PLT/GPLT formulation, the virtual measurements are utilized to provide assisted measurement inputs while the signal sources are insufficient. Associating with the designed set of virtual BSs $\boldsymbol{P}_{BS_v,k}$, the corresponding set of virtual measurements $\boldsymbol{r}_{v,k}$ is defined as*

$$\boldsymbol{r}_{v,k} = \begin{cases} \{r_{v_1,k}\}, & for\ N_k = 2 \\ \{r_{v_1,k},\ r_{v_2,k}\}, & for\ N_k = 1. \end{cases} \tag{6}$$

It is noticed that the major tasks of both the PLT and GPLT schemes are to design and to acquire the values of $\boldsymbol{P}_{BS_v,k}$ and $\boldsymbol{r}_{v,k}$ for the two cases (i.e., $N_k = 1$ and 2) with inadequate signal sources. In both the KT and CLT schemes, the estimated state vector $\hat{\boldsymbol{s}}_k$ can only be updated by the internal prediction mechanism of the Kalman filter while there are insufficient numbers of BSs (i.e., $N_k < 3$, as shown in Figs. 1a and 1b with the dashed lines). The location estimator (i.e., the two-step LS method) is, consequently, disabled owing to the inadequate number of the signal sources. The tracking capabilities of both schemes significantly depend on the correctness of the Kalman filter's prediction mechanism. Therefore, the performance for location tracking can be severely degraded due to the changing behavior of the MS, i.e., with the variations from the MS's acceleration.

On the other hand, the proposed PLT/GPLT algorithms can still provide satisfactory tracking performance with deficient measurement inputs, i.e., with $N_k = 1$ and 2. Under these circumstances, the location estimator is still effective with the additional virtual BSs $\boldsymbol{P}_{BS_v,k}$ and the virtual measurements $\boldsymbol{r}_{v,k}$, which are imposed from the predictive output of the Kalman filter (as shown in Fig. 1c). It is also noted that the PLT/GPLT schemes will perform the same as the CLT method under the case with no signal input, i.e., under $N_k = 0$. Furthermore, the GPLT algorithm enhances the precision and the robustness of the location estimation from the PLT scheme by considering the GDOP effect, i.e., the geographic relationship between the locations of the BSs and the MS. By adopting the GPLT scheme, the locations of the virtual BSs $\boldsymbol{P}^{PLT}_{BS_v,k}$ obtained from the PLT method are adjusted into $\boldsymbol{P}^{GPLT}_{BS_v,k}$ in order that the predicted MS has minimal GDOP value. Consequently, smaller estimation errors can be acquired by exploiting the GPLT algorithm compared with the PLT scheme. The virtual BS's location set $\boldsymbol{P}^{PLT}_{BS_v,k}$ and the virtual measurements $\boldsymbol{r}^{PLT}_{v,k}$ by exploiting the PLT formulation are presented in the next section; while the adjusted location set of the virtual BSs $\boldsymbol{P}^{GPLT}_{BS_v,k}$ adopted from the GPLT algorithm will be derived in Section 5.

4 Formulation of PLT Algorithm

The proposed PLT scheme will be explained in this section. As shown in Fig. 1c, the measurement and state equations for the Kalman filter can be represented as

$$\boldsymbol{z}_k = \mathbf{M}\hat{\boldsymbol{s}}_k + \boldsymbol{m}_k, \tag{7}$$

$$\hat{\boldsymbol{s}}_k = \mathbf{F}\hat{\boldsymbol{s}}_{k-1} + \boldsymbol{p}_k, \tag{8}$$

where $\hat{\boldsymbol{s}}_k = [\hat{\boldsymbol{x}}_k\ \hat{\boldsymbol{v}}_k\ \hat{\boldsymbol{a}}_k]^T$. The variables $\boldsymbol{m}_k$ and $\boldsymbol{p}_k$ denote the measurement and the process noises associated with the covariance matrices $\mathbf{R}$ and $\mathbf{Q}$ within the Kalman filtering formulation. The measurement vector $\boldsymbol{z}_k = [\hat{x}_{ls,k}\ \hat{y}_{ls,k}]^T$ represents the measurement input which is obtained from the output of the two-step LS estimator at the kth time step (as

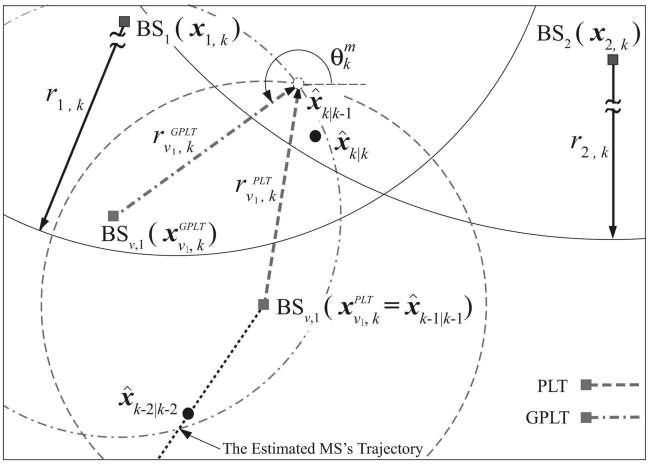

Fig. 2. The schematic diagram of the two-BSs case for the proposed PLT and GPLT schemes.

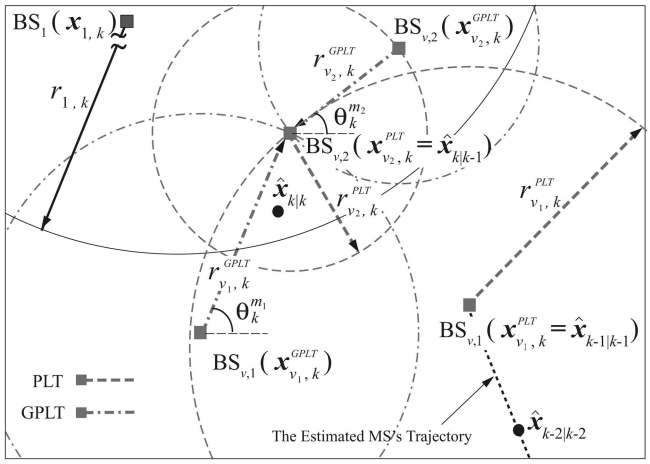

Fig. 3. The schematic diagram of the single-BS case for the proposed PLT and GPLT schemes.

in Fig. 1c). The matrix $\mathbf{M}$ and the state transition matrix $\mathbf{F}$ can be obtained as

$$\mathbf{M} = \begin{bmatrix} 1 & 0 & 0 & 0 & 0 & 0 \\ 0 & 1 & 0 & 0 & 0 & 0 \end{bmatrix}, \tag{9}$$

$$\mathbf{F} = \begin{bmatrix} 1 & 0 & \Delta t & 0 & \frac{1}{2}\Delta t^2 & 0 \\ 0 & 1 & 0 & \Delta t & 0 & \frac{1}{2}\Delta t^2 \\ 0 & 0 & 1 & 0 & \Delta t & 0 \\ 0 & 0 & 0 & 1 & 0 & \Delta t \\ 0 & 0 & 0 & 0 & 1 & 0 \\ 0 & 0 & 0 & 0 & 0 & 1 \end{bmatrix}, \tag{10}$$

where Δt denotes the sample time interval. The main concept of the PLT scheme is to provide additional virtual measurements (i.e., $\boldsymbol{r}_{v,k}$ as in (6)) to the two-step LS estimator while the signal sources are insufficient. Two cases (i.e., the two-BSs case and the single-BS case) are considered as given below.

4.1 Two-BSs Case

As shown in Fig. 2, it is assumed that only two BSs (i.e., BS_1 and BS_2) associated with two TOA measurements are available at the time step k in consideration. The main target is to introduce an additional virtual BS along with its virtual measurement (i.e., $\boldsymbol{P}^{PLT}_{BS_v,k} = \{\boldsymbol{x}^{PLT}_{v_1,k}\}$ and $\boldsymbol{r}^{PLT}_{v,k} = \{r^{PLT}_{v_1,k}\}$) by acquiring the predictive output information from the Kalman filter. Knowing that there are predicting and correcting phases within the Kalman filtering formulation, the predictive state can, therefore, be utilized to compute the supplementary virtual measurement $r^{PLT}_{v_1,k}$ as

$$\begin{aligned} r^{PLT}_{v_1,k} &= \|\hat{\boldsymbol{x}}_{k|k-1} - \hat{\boldsymbol{x}}_{k-1|k-1}\| \\ &= \|\mathbf{MF}\ \hat{\boldsymbol{s}}_{k-1|k-1} - \hat{\boldsymbol{x}}_{k-1|k-1}\|, \end{aligned} \tag{11}$$

where $\hat{\boldsymbol{x}}_{k|k-1}$ denotes the predicted MS's position at time step k; while $\hat{\boldsymbol{x}}_{k-1|k-1}$ is the corrected (i.e., estimated) MS's position obtained at the $(k-1)$th time step. It is noticed that both values are available at the $(k-1)$th time step. The virtual measurement $r^{PLT}_{v_1,k}$ is defined as the distance between the previous location estimate ($\hat{\boldsymbol{x}}_{k-1|k-1}$) as the position of the virtual BS (i.e., $\mathrm{BS}_{v,1}$: $\boldsymbol{x}^{PLT}_{v_1,k} \triangleq \hat{\boldsymbol{x}}_{k-1|k-1}$) and the predicted MS's position ($\hat{\boldsymbol{x}}_{k|k-1}$) as the possible position of the MS (as shown in Fig. 2). It is also noted that the corrected state vector $\hat{\boldsymbol{s}}_{k-1|k-1}$ is available at the current time step k. However, due to the insufficient measurement input, the state vector $\hat{\boldsymbol{s}}_{k|k}$ is unobtainable at the kth time step while adopting the conventional two-step LS estimator. By exploiting $r^{PLT}_{v_1,k}$ (in (11)) as the additional signal input, the measurement vector $\boldsymbol{z}_k$ can be acquired after the three measurement inputs $\boldsymbol{r}^e_k = \{r_{1,k},\ r_{2,k},\ r^{PLT}_{v_1,k}\}$ and the locations of the BSs $\boldsymbol{P}^e_{BS,k} = \{\boldsymbol{x}_{1,k},\ \boldsymbol{x}_{2,k},\ \boldsymbol{x}^{PLT}_{v_1,k}\}$ have been imposed into the two-step LS estimator. As $\boldsymbol{z}_k$ has been obtained, the corrected state vector $\hat{\boldsymbol{s}}_{k|k}$ can be updated with the implementation of the correcting phase of the Kalman filter at the time step k as

$$\begin{aligned} \hat{\boldsymbol{s}}_{k|k} =& \hat{\boldsymbol{s}}_{k|k-1} + \mathbf{P}_{k|k-1}\mathbf{M}^T[\mathbf{M}\mathbf{P}_{k|k-1}\mathbf{M}^T + \mathbf{R}]^{-1} \\ & \cdot (\boldsymbol{z}_k - \mathbf{M}\hat{\boldsymbol{s}}_{k|k-1}), \end{aligned} \tag{12}$$

where

$$\mathbf{P}_{k|k-1} = \mathbf{F}\mathbf{P}_{k-1|k-1}\mathbf{F}^T + \mathbf{Q} \tag{13}$$

and

$$\begin{aligned} \mathbf{P}_{k-1|k-1} =& [\ \mathbf{I} - \mathbf{P}_{k-1|k-2}\mathbf{M}^T\ (\mathbf{M}\mathbf{P}_{k-1|k-2}\mathbf{M}^T + \mathbf{R})^{-1}\mathbf{M}\ ] \\ & \cdot\ \mathbf{P}_{k-1|k-2.} \end{aligned} \tag{14}$$

It is noted that $\mathbf{P}_{k|k-1}$ and $\mathbf{P}_{k-1|k-1}$ represent the predicted and the corrected estimation covariance within the Kalman filter. $\mathbf{I}$ in (14) is denoted as an identity matrix. As can be observed from Fig. 2, the virtual measurement $r^{PLT}_{v_1,k}$ associated with the other two existing measurements $r_{1,k}$ and $r_{2,k}$ provide a confined region for the estimation of the MS's location at the time step k, i.e., $\hat{\boldsymbol{x}}_{k|k}$.

4.2 Single-BS Case

In this case, only one BS (i.e., BS_1) with one TOA measurement input is available at the kth time step (as shown in Fig. 3). Two additional virtual BSs and measurements are

required for the computation of the two-step LS estimator, i.e., $\boldsymbol{P}_{BS_v,k}^{PLT} = \{\boldsymbol{x}_{v_1,k}^{PLT},\ \boldsymbol{x}_{v_2,k}^{PLT}\}$ and $\boldsymbol{r}_{v,k}^{PLT} = \{r_{v_1,k}^{PLT},\ r_{v_2,k}^{PLT}\}$. Similar to the previous case, the first virtual measurement $r_{v_1,k}^{PLT}$ is acquired as in (11) by considering $\hat{\boldsymbol{x}}_{k-1|k-1}$ as the position of the first virtual BS (i.e., $\boldsymbol{x}_{v_1,k}^{PLT} = \hat{\boldsymbol{x}}_{k-1|k-1}$) with the predicted MS's position (i.e., $\hat{\boldsymbol{x}}_{k|k-1}$) as the possible position of the MS. On the other hand, the second virtual BS's position is assumed to locate at the predicted MS's position (i.e., $\boldsymbol{x}_{v_2,k}^{PLT} \triangleq \hat{\boldsymbol{x}}_{k|k-1}$), as illustrated in Fig. 3. The corresponding second virtual measurement $r_{v_2,k}^{PLT}$ is defined as the average prediction error obtained from the Kalman filtering formulation by accumulating the previous time steps as

$$r_{v_2,k}^{PLT} = \frac{1}{k-1}\sum_{i=1}^{k-1} \|\hat{\boldsymbol{x}}_{i|i} - \hat{\boldsymbol{x}}_{i|i-1}\|. \tag{15}$$

It is noted that $r_{v_2,k}^{PLT}$ is obtained as the mean prediction error until the $(k-1)$th time step. In the case while the Kalman filter is capable of providing sufficient accuracy in its prediction phase, the virtual measurement $r_{v_2,k}^{PLT}$ may approach zero value. Associated with the single measurement $r_{1,k}$ from BS_1, the two additional virtual measurements $r_{v_1,k}^{PLT}$ (centered at $\hat{\boldsymbol{x}}_{k-1|k-1}$) and $r_{v_2,k}^{PLT}$ (centered at $\hat{\boldsymbol{x}}_{k|k-1}$) result in a constrained region (as in Fig. 3) for location estimation of the MS under the environments with insufficient signal sources.

It is also noticed that the variations of the measurement inputs are the required information for adopting the two-step LS estimator. It utilizes the signal variation as an indicator to consider the weighting factor for a specific signal source, i.e., smaller weighting coefficient should be assigned to a measurement input if it encompasses comparably larger signal variations. The weighted least-square algorithm can, therefore, be performed within the two-step LS estimator according to the designated weighting values associated with the signal sources. A similar concept can be exploited to assign the weighting coefficients for the virtual measurements. The virtual measurements can be represented as

$$r_{v_i,k} = \zeta_{v_i,k} + n_{v_i,k}, \quad \text{for } i = 1, 2, \tag{16}$$

where $\zeta_{v_i,k}$ is denoted as the deterministic noiseless virtual measurement; while $n_{v_i,k}$ represents the *virtual noise* (i.e., the component with randomness) associated with the virtual measurement $r_{v_i,k}$. The following Lemma illustrates that the resultant virtual noises $n_{v_i,k}$ are considered zero-mean random variables.

Lemma 1. *Based on the definition of the virtual measurements $r_{v_i,k}^{PLT}$, as in (11) and (15), the corresponding virtual noises become zero-mean random variables.*

Proof. The first virtual measurement $r_{v_1,k}^{PLT}$, as proposed in (11), is considered first. Based on (16), the virtual noise $n_{v_1,k}^{PLT}$ associated with $r_{v_1,k}^{PLT}$ can be written as

$$\begin{aligned} n_{v_1,k}^{PLT} &= r_{v_i,k}^{PLT} - \zeta_{v_i,k}^{PLT} \\ &= \|\hat{\boldsymbol{x}}_{k|k-1} - \hat{\boldsymbol{x}}_{k-1|k-1}\| - \|\boldsymbol{x}_k - \hat{\boldsymbol{x}}_{k-1|k-1}\|. \end{aligned} \tag{17}$$

It is noted that both the variables $\hat{\boldsymbol{x}}_{k|k-1}$ and $\hat{\boldsymbol{x}}_{k-1|k-1}$ are acquired from the Kalman filtering formulation. The primary target of the Kalman filter is to achieve zero-mean estimation errors, i.e., $E[\boldsymbol{x}_k - \hat{\boldsymbol{x}}_{k|k}] = E[\boldsymbol{x}_k - \hat{\boldsymbol{x}}_{k|k-1}] = 0$. It can, consequently, be obtained that $E[\boldsymbol{x}_k] = E[\hat{\boldsymbol{x}}_{k|k}] = E[\hat{\boldsymbol{x}}_{k|k-1}]$ as the estimation errors converge. Considering that the variables $\boldsymbol{x}_k, \hat{\boldsymbol{x}}_{k|k}$, and $\hat{\boldsymbol{x}}_{k|k-1}$ possess the same probability distribution, the expected value of the first virtual noise can, therefore, be rewritten as

$$\begin{aligned} E\big[n_{v_1,k}^{PLT}\big] &= E[\|\hat{\boldsymbol{x}}_{k|k-1} - \hat{\boldsymbol{x}}_{k-1|k-1}\|] - E[\|\boldsymbol{x}_k - \hat{\boldsymbol{x}}_{k-1|k-1}\|] \\ &= \|E[\hat{\boldsymbol{x}}_{k|k-1}] - E[\hat{\boldsymbol{x}}_{k-1|k-1}]\| - \|E[\boldsymbol{x}_k] - E[\hat{\boldsymbol{x}}_{k-1|k-1}]\| \\ &= \|E[\boldsymbol{x}_k] - E[\hat{\boldsymbol{x}}_{k-1|k-1}]\| - \|E[\boldsymbol{x}_k] - E[\hat{\boldsymbol{x}}_{k-1|k-1}]\| = 0. \end{aligned}$$

The result shows that the first virtual measurement $r_{v_i,k}^{PLT}$ has virtual noise $n_{v_1,k}^{PLT}$ with zero-mean value.

Similarly, the virtual noise $n_{v_2,k}^{PLT}$ associated with the second virtual measurement $r_{v_2,k}^{PLT}$ (in (15)) can be expressed as

$$\begin{aligned} n_{v_2,k}^{PLT} &= r_{v_2,k}^{PLT} - \zeta_{v_2,k}^{PLT} \\ &= \left[\frac{1}{k-1}\sum_{i=1}^{k-1} \|\hat{\boldsymbol{x}}_{i|i} - \hat{\boldsymbol{x}}_{i|i-1}\|\right] - \|\boldsymbol{x}_k - \hat{\boldsymbol{x}}_{k|k-1}\|. \end{aligned} \tag{18}$$

Based on the same estimation objective by adopting the Kalman filter, the expected value of the virtual noise $n_{v_2,k}^{PLT}$ is obtained as

$$\begin{aligned} E\big[n_{v_2,k}^{PLT}\big] &= \frac{1}{k-1}\sum_{i=1}^{k-1} E[\|\hat{\boldsymbol{x}}_{i|i} - \hat{\boldsymbol{x}}_{i|i-1}\|] - E[\|\boldsymbol{x}_k - \hat{\boldsymbol{x}}_{k|k-1}\|] \\ &= \frac{1}{k-1}\sum_{i=1}^{k-1} \|E[\hat{\boldsymbol{x}}_{i|i}] - E[\hat{\boldsymbol{x}}_{i|i-1}]\| \\ &\quad - \|E[\boldsymbol{x}_k] - E[\hat{\boldsymbol{x}}_{k|k-1}]\| = 0. \end{aligned}$$

The result indicates that the virtual noise $n_{v_2,k}^{PLT}$ associated with the second virtual measurement is acquired as a zero-mean random variable. This completes the proof. □

It is noticed that the zero-mean characteristics of the virtual noises (as was proved in Lemma 1) will be utilized as a property for Lemma 2 in the next section. Based on (11), the signal variation of $r_{v_1,k}^{PLT}$ is considered as the variance of the predicted distance $\|\hat{\boldsymbol{x}}_{k|k-1} - \hat{\boldsymbol{x}}_{k-1|k-1}\|$ between the previous $(k-1)$ time steps. Associated with the result obtained from Lemma 1, the virtual noise $n_{v_1,k}$ is regarded as zero mean with variance $\sigma_{n_{v_1,k}}^2 = \mathrm{Var}(r_{v_1,k}^{PLT}) = \mathrm{Var}(\|\hat{\boldsymbol{x}}_{k|k-1} - \hat{\boldsymbol{x}}_{k-1|k-1}\|)$. Similarly, since the signal variation of the second virtual measurement $r_{v_2,k}^{PLT}$ is obtained as the variance of the averaged prediction errors (as in (15)), the associated virtual noise $n_{v_2,k}$ can also be considered as zero mean with variance $\sigma_{n_{v_2,k}}^2 = \mathrm{Var}(r_{v_2,k}^{PLT})$. Consequently, the variances of the virtual noises (i.e., $\sigma_{n_{v_1,k}}^2$ and $\sigma_{n_{v_2,k}}^2$) will be exploited as the weighting coefficients within the formulation of the two-step LS estimator.

5 Formulation of GPLT Algorithm

As was explained in Section 2.3, the geometric relationship between the MS and its associated BSs (i.e., indicated by the

corresponding GDOP value) will affect the precision for location estimation and tracking. The concept of the proposed GPLT scheme is to adjust the positions of the virtual BSs such that the predicted MS will, consequently, be possessed with a smaller GDOP value based on the newly formed geometric layout. The modified positions of the virtual BSs will, therefore, be adopted associated with the existing BSs for location estimation. Similarly, the two-BSs and the single-BS cases are considered for the GPLT algorithm as given below.

5.1 Two-BSs Case

In this case, the primary target for the GPLT scheme is to design the location of the virtual BS, i.e., $\mathrm{BS}_{v,1}$: $\boldsymbol{x}_{v_1,k}^{GPLT}$. As shown in Fig. 2, two parameters (i.e., the distance $r_{v_1,k}^{GPLT}$ and the angle θ_k) w.r.t. the predicted MS's position $\hat{\boldsymbol{x}}_{k|k-1}$ are introduced to represent the designed virtual BS's position $\boldsymbol{x}_{v_1,k}^{GPLT}$. The selection of these two parameters within the GPLT algorithm is explained in the following sections.

5.1.1 Computation of Angle θ_k

The main objective of the GPLT scheme is to acquire the angle θ_k of $\boldsymbol{x}_{v_1,k}^{GPLT}$ such that the predicted MS ($\hat{\boldsymbol{x}}_{k|k-1}$) will possess a minimal GDOP value within its network topology for location estimation. As illustrated in Fig. 2, the following equality can be obtained based on the geometric relationship:

$$\hat{\boldsymbol{x}}_{k|k-1} - \boldsymbol{x}_{v_1,k}^{GPLT} = \left(-r_{v_1,k}^{GPLT} \cdot \cos\theta_k,\ -r_{v_1,k}^{GPLT} \cdot \sin\theta_k\right). \quad (19)$$

It is noticed that the angle θ_k is rotated from the positive x-axis based on the predicted MS ($\hat{\boldsymbol{x}}_{k|k-1}$). As mentioned above, the position of the virtual BS ($\boldsymbol{x}_{v_1,k}^{GPLT}$) is designed such that the predicted MS ($\hat{\boldsymbol{x}}_{k|k-1}$) will be located at a minimal GDOP position based on the extended geometric set $\boldsymbol{P}_{BS,k}^{e} = \{\boldsymbol{x}_{1,k},\ \boldsymbol{x}_{2,k},\ \boldsymbol{x}_{v_1,k}^{GPLT}\}$. By incorporating (19) into (3) and (4), the GDOP value (i.e., $\mathrm{G}_{\hat{\boldsymbol{x}}_{k|k-1}}$) computed at the predicted MS's position $\hat{\boldsymbol{x}}_{k|k-1} = (\hat{x}_{k|k-1},\ \hat{y}_{k|k-1})$ can be obtained. The associated matrix $\mathbf{H}_{\hat{\boldsymbol{x}}_{k|k-1}}$ becomes

$$\begin{aligned}\mathbf{H}_{\hat{\boldsymbol{x}}_{k|k-1}} &= \begin{bmatrix} \frac{\hat{x}_{k|k-1}-x_{1,k}}{r_{1,k}} & \frac{\hat{y}_{k|k-1}-y_{1,k}}{r_{1,k}} \\ \frac{\hat{x}_{k|k-1}-x_{2,k}}{r_{2,k}} & \frac{\hat{y}_{k|k-1}-y_{2,k}}{r_{2,k}} \\ \frac{\hat{x}_{k|k-1}-x_{v_1,k}^{GPLT}}{r_{v_1,k}^{GPLT}} & \frac{\hat{y}_{k|k-1}-y_{v_1,k}^{GPLT}}{r_{v_1,k}^{GPLT}} \end{bmatrix} \\ &= \begin{bmatrix} \frac{\hat{x}_{k|k-1}-x_{1,k}}{r_{1,k}} & \frac{\hat{y}_{k|k-1}-y_{1,k}}{r_{1,k}} \\ \frac{\hat{x}_{k|k-1}-x_{2,k}}{r_{2,k}} & \frac{\hat{y}_{k|k-1}-y_{2,k}}{r_{2,k}} \\ -\cos\theta_k & -\sin\theta_k \end{bmatrix}. \end{aligned} \quad (20)$$

It is noted that the noiseless relative distances $\zeta_{i,k}$ in (3) are approximately replaced by $r_{i,k}$ in (20) since $\zeta_{i,k}$ are considered unattainable. It can be observed from (20) that the matrices $\mathbf{H}_{\hat{\boldsymbol{x}}_{k|k-1}}$ associated with the resulting $\mathrm{G}_{\hat{\boldsymbol{x}}_{k|k-1}}$ values are regarded as functions of the angle θ_k, i.e., $\mathbf{H}_{\hat{\boldsymbol{x}}_{k|k-1}}(\theta_k)$ and $\mathrm{G}_{\hat{\boldsymbol{x}}_{k|k-1}}(\theta_k)$. Based on the objective of the GPLT scheme, the angle θ_k^m which results in the minimal GDOP value can, therefore, be acquired as

$$\theta_k^m = \arg\left\{\min_{\forall\theta_k} \mathrm{G}_{\hat{\boldsymbol{x}}_{k|k-1}}(\theta_k)\right\}. \quad (21)$$

It is intuitive to observe that (21) can be achieved if the following conditions on the first and second derivatives of $\mathrm{G}_{\hat{\boldsymbol{x}}_{k|k-1}}(\theta_k)$ are satisfied:

$$\left[\frac{\partial \mathrm{G}_{\hat{\boldsymbol{x}}_{k|k-1}}(\theta_k)}{\partial\theta_k}\right]_{\theta_k=\theta_k^m} = 0, \quad (22)$$

$$\left[\frac{\partial^2 \mathrm{G}_{\hat{\boldsymbol{x}}_{k|k-1}}(\theta_k)}{\partial {\theta_k}^2}\right]_{\theta_k=\theta_k^m} > 0. \quad (23)$$

By substituting (20) and (3) into (22), the angle θ_k^m can be computed as

$$\theta_k^m = \tan^{-1}\left(\frac{1 \pm \sqrt{1+\Gamma^2}}{\Gamma}\right), \quad (24)$$

where

$$\begin{aligned}\Gamma = \{&2[r_{2,k}^2(\hat{x}_{k|k-1}-x_{1,k})(\hat{y}_{k|k-1}-y_{1,k}) \\ &+ r_{1,k}^2(\hat{x}_{k|k-1}-x_{2,k})(\hat{y}_{k|k-1}-y_{2,k})]\} \\ &/\{r_{2,k}^2(\hat{x}_{k|k-1}-x_{1,k})^2 - r_{2,k}^2(\hat{y}_{k|k-1}-y_{1,k})^2 \\ &+ r_{1,k}^2(\hat{x}_{k|k-1}-x_{2,k})^2 - r_{1,k}^2(\hat{y}_{k|k-1}-y_{2,k})^2\}.\end{aligned} \quad (25)$$

It is noted that the selection for either the positive or the negative value of θ_k^m is determined by (23). At each time instant k, the relative angle θ_k^m between $\hat{\boldsymbol{x}}_{k|k-1}$ and $\boldsymbol{x}_{v_1,k}^{GPLT}$ can, therefore, be obtained such that $\hat{\boldsymbol{x}}_{k|k-1}$ is located at the position with a minimal GDOP value based on its current network layout.

Moreover, it is important to observe from (24) and (25) that the angle θ_k^m is independent of the virtual measurement $r_{v_1,k}^{GPLT}$. In other words, considering the two-BS case with one adjustable virtual BS, the distance $r_{v_1,k}^{GPLT}$ can, arbitrarily, be chosen along the direction with angle θ_k^m and, consequently, the minimal GDOP for $\hat{\boldsymbol{x}}_{k|k-1}$ is still attained. However, this result does not guarantee the independency between the virtual distance $r_{v_1,k}^{GPLT}$ and the estimation errors. In the next section, the distance effect to the location estimation errors will further be evaluated.

5.1.2 Selection of Distance $r_{v_1,k}^{GPLT}$

In this section, the virtual measurement $r_{v_1,k}^{GPLT}$ will be determined, which can be utilized for acquiring the position of the virtual BS $\boldsymbol{x}_{v_1,k}^{GPLT}$. It is observed in (20) that the GDOP value at the predicted MS's position is primarily dominated by the relative angle (i.e., θ_k) between the MS and the BSs; while the distance information (i.e., $r_{v_1,k}^{GPLT}$) is considered uninfluential to the GDOP value. This uncorrelated relationship between the GDOP value and the relative distance has also been observed, as in [25]. The following Lemma shows that the selection of the virtual distance $r_{v_1,k}^{GPLT}$ becomes insignificant for the WLS-based location estimation.

Lemma 2. *A time-based location estimation problem is considered for the MS using the Weighted Least-Square (WLS) algorithm. Assuming that a measurement input obtained from a specific BS is associated with zero-mean random noises, the expected*

value of the location estimation error is independent of the distance between the specific BS and the MS.

The proof of Lemma 2 is shown in the Appendix. This lemma states that the expected value of the location estimation error is independent of the distance between a specific BS to the MS if the noises associated with the measurement inputs are statistically distributed with a zero-mean value. In generic time-based location estimation, the phenomenon stated in Lemma 2 does not usually exist since most of the measurement inputs are contaminated with NLOS noises, i.e., $e_{i,k}$ in (1) is randomly distributed with positive mean value. The NLOS error is augmented as the distance between the specific BS and the MS is increased, which causes the corresponding measurement input to become unreliable compared with the other signal sources. This result is consistent with the intuition that BSs with closer distances to the MS are always selected for location estimation. In the proposed GPLT scheme, however, the virtual measurement $r_{v_1,k}^{GPLT}$ is considered as a designed distance which is infected by its corresponding virtual noise $n_{v_1,k}^{GPLT}$ with zero mean value (as can be obtained from Lemma 1). Based on Lemma 2, the selection of the distance $r_{v_1,k}^{GPLT}$ becomes uninfluential to the estimation error while exploiting the WLS algorithm for location estimation. This result is similar to the derived GDOP value that is unrelated to the distance information between the BSs and the MS (as can be observed from (20)). In the simulation section, the uncorrelated relationship between $r_{v_1,k}^{GPLT}$ and the estimation error will further be validated by exploiting the two-step LS estimator, which is considered one of the the WLS-based algorithms for location estimation. It will be demonstrated via the simulation results that the influence from the length of the virtual measurement to the estimation error is considered insignificant.

The procedures of the proposed GPLT scheme under the two-BSs case is explained as follows: The target is to obtain the position of the MS at the kth time step (i.e., $\hat{\boldsymbol{x}}_{k|k}$) based on the available information, including the measurement and location information acquired from both BS_1 and BS_2 along with the predicted position of the MS (i.e., $\hat{\boldsymbol{x}}_{k|k-1}$). Two steps are involved within the proposed GPLT scheme: 1) the determination of the virtual BS's position and the virtual measurement and 2) the estimation and tracking of the MS's position. As shown in Fig. 2, the orientation of the virtual BS (θ_k^m) relative to the predicted MS's position $\hat{\boldsymbol{x}}_{k|k-1}$ is determined based on the criterion of minimizing the GDOP value on $\hat{\boldsymbol{x}}_{k|k-1}$ (as obtained from (21) and (24)). As was indicated by Lemma 2, the selection of the virtual distance $r_{v_1,k}^{GPLT}$ w.r.t. the predicted MS's position $\hat{\boldsymbol{x}}_{k|k-1}$ is considered insignificant to the estimation errors. Therefore, the distance is selected the same value as was designed in the PLT algorithm, i.e., $r_{v_1,k}^{GPLT} = r_{v_1,k}^{PLT}$, as in (11). The location of the virtual BS ($\boldsymbol{x}_{v_1,k}^{GPLT}$) and the length of the virtual measurement ($r_{v_1,k}^{GPLT}$) can, consequently, be acquired. It is also noticed that the design of the virtual noise can, therefore, be selected the same as that in the PLT scheme, i.e., zero-mean random distributed with variance $\sigma_{n_{v_1,k}}^2 = \mathrm{Var}(r_{v_1,k}^{PLT}) = \mathrm{Var}(\|\hat{\boldsymbol{x}}_{k|k-1} - \hat{\boldsymbol{x}}_{k-1|k-1}\|)$.

After acquiring the information of the virtual BS as the additional signal source, the extended sets of the BSs and the measurement inputs can be established as $\boldsymbol{P}_{BS,k}^e = \{\boldsymbol{x}_{1,k}, \boldsymbol{x}_{2,k}, \boldsymbol{x}_{v_1,k}^{GPLT}\}$ and $\boldsymbol{r}_k^e = \{r_{1,k}, r_{2,k}, r_{v_1,k}^{GPLT}\}$. As illustrated in Fig. 1c, the extended set of signal sources is utilized as the input to the two-step LS estimator. The estimated MS's position $\hat{\boldsymbol{x}}_{k|k}$ can, therefore, be obtained by adopting the correcting phase of the Kalman filter, which completes the location estimation and tracking processes at the kth time step.

5.2 Single-BS Case

As illustrated in Fig. 3, only one BS ($\boldsymbol{x}_{1,k}$) associated with the measurement input $r_{1,k}$ is available at the considered kth time instant. Additional two virtual BSs associated with their virtual measurements are required as the inputs for the two-step LS estimator, i.e., $\boldsymbol{P}_{BS_v,k}^{GPLT} = \{\boldsymbol{x}_{v_1,k}^{GPLT}, \boldsymbol{x}_{v_2,k}^{GPLT}\}$ and $\boldsymbol{r}_{v,k}^{GPLT} = \{r_{v_1,k}^{GPLT}, r_{v_2,k}^{GPLT}\}$. By adopting a similar concept as stated in Section 5.1, the following equations can be obtained based on the geometric relationships from Fig. 3:

$$\hat{\boldsymbol{x}}_{k|k-1} - \boldsymbol{x}_{v_1,k}^{GPLT} = \left(-r_{v_1,k}^{GPLT} \cdot \cos\theta_k^{m_1},\ -r_{v_1,k}^{GPLT} \cdot \sin\theta_k^{m_1}\right), \quad (26)$$

$$\hat{\boldsymbol{x}}_{k|k-1} - \boldsymbol{x}_{v_2,k}^{GPLT} = \left(-r_{v_2,k}^{GPLT} \cdot \cos\theta_k^{m_2},\ -r_{v_2,k}^{GPLT} \cdot \sin\theta_k^{m_2}\right). \quad (27)$$

Based on (26) and (27), it can be observed that the design concept of the GPLT scheme for the single-BS case is to obtain the feasible locations for both $\boldsymbol{x}_{v_1,k}^{GPLT}$ and $\boldsymbol{x}_{v_2,k}^{GPLT}$ by rotating around the predicted MS's location $\hat{\boldsymbol{x}}_{k|k-1}$. For fair comparison, the two virtual measurements are designed to be the same as that utilized in the PLT scheme, i.e., $\boldsymbol{r}_{v,k}^{GPLT} = \{r_{v_1,k}^{PLT}, r_{v_2,k}^{PLT}\}$, as in (11) and (15). The two rotating angles $\theta_k^{m_1}$ and $\theta_k^{m_2}$ that are designed to be hinged at the predicted MS's location $\hat{\boldsymbol{x}}_{k|k-1}$ will be sequentially determined as follows: First of all, as shown in Fig. 3, the position of the second virtual BS ($\boldsymbol{x}_{v_2,k}^{GPLT}$) is designed at a location with distance $r_{v_2,k}^{GPLT}$ relative to the predicted MS's position $\hat{\boldsymbol{x}}_{k|k-1}$. It is noted that the position of the first virtual BS that is designed from the PLT scheme (i.e., $\boldsymbol{x}_{v_1,k}^{PLT} = \hat{\boldsymbol{x}}_{k-1|k-1}$) is assigned as the preliminary position for the first virtual BS, i.e., $\boldsymbol{x}_{v_1,k}^{GPLT} = \boldsymbol{x}_{v_1,k}^{PLT}$. Based on the information acquired from $\mathrm{BS}_1(\boldsymbol{x}_{1,k})$ and $\boldsymbol{x}_{v_1,k}^{PLT}$ associated with the predicted MS's position $\hat{\boldsymbol{x}}_{k|k-1}$, the rotating angle $\theta_k^{m_2}$ for the second virtual BS can be acquired, as in (24). After the angle $\theta_k^{m_2}$ has been obtained, the position of the second virtual BS ($\boldsymbol{x}_{v_2,k}^{GPLT}$) becomes available, as in (27). The same procedure, based on (24), can be adopted to obtain the rotating angle $\theta_k^{m_1}$ of the first virtual BS, where the available information includes $\boldsymbol{x}_{1,k}$ and $\boldsymbol{x}_{v_2,k}^{GPLT}$ associated with the predicted MS's position $\hat{\boldsymbol{x}}_{k|k-1}$. Consequently, the positions for both of the virtual measurements $\boldsymbol{x}_{v_1,k}^{GPLT}$ and $\boldsymbol{x}_{v_2,k}^{GPLT}$ can be determined.

Based on intuitive observation and the computation of GDOP value from (3), a comparable larger GDOP occurs if the geometric layout formed by the three BSs is approximately collinear, i.e., less than 5 degree in one of the triangular

angles. This situation, in general, happens by adopting the PLT scheme under the single-BS case, especially under the situation while the MS is moving along the same direction for a certain time interval. As shown in Fig. 3, the designed positions of the virtual BSs, i.e., $\boldsymbol{x}_{v_1,k}^{PLT}$ and $\boldsymbol{x}_{v_2,k}^{PLT}$, are observed to be collinear with the measurement input $\mathrm{BS}_1(\boldsymbol{x}_{1,k})$. The benefits of exploiting the GPLT scheme can be revealed in consideration of the collinearity problem. With the computation of the angle $\theta_k^{m_2}$ from the GPLT scheme, the collinear situation between BS_1 and $\mathrm{BS}_{v,2}$ can be avoided; while the rotated angle $\theta_k^{m_1}$ alleviates the potential small angle between BS_1 and $\mathrm{BS}_{v,1}$. By considering the geometric layout within the design of the GPLT scheme, the situations with worse GDOP value can be improved. The precision for location estimation and tracking of the MS can, consequently, be enhanced.

6 Performance Evaluation

Simulations are performed to show the effectiveness of the proposed PLT and GPLT schemes under different numbers of BSs, including the scenarios with deficient signal sources. The noise models and the simulation parameters are illustrated in Section 6.1. Section 6.2 validates the GPLT scheme according to the variations from the relative angle and the distance between the MS and the designed virtual BS. The performance comparison between the proposed PLT and GPLT algorithms with the other existing location tracking schemes, i.e., the KT and the CLT techniques, are conducted in Section 6.3.

6.1 Noise Models and Simulation Parameters

Different noise models [32], [33] for the TOA measurements are considered in the simulations. The model for the measurement noise of the TOA signals is selected as the Gaussian distribution with zero mean and 10 meters of standard deviation, i.e., $n_{i,k} \sim \mathcal{N}(0, 100)$. On the other hand, an exponential distribution $p_{e_{i,k}}(\upsilon)$ is assumed for the NLOS noise model of the TOA measurements as

$$p_{e_{i,k}}(\upsilon) = \begin{cases} \frac{1}{\lambda_{i,k}} \exp\left(-\frac{\upsilon}{\lambda_{i,k}}\right), & \upsilon > 0 \\ 0, & \text{otherwise}, \end{cases} \tag{28}$$

where $\lambda_{i,k} = c \cdot \tau_{i,k} = c \cdot \tau_m(\zeta_{i,k})^{\varepsilon} \rho$. The parameter $\tau_{i,k}$ is the RMS delay spread between the ith BS to the MS. τ_m represents the median value of $\tau_{i,k}$, which is selected as $0.1\ \mu s$ in the simulations. ε is the path loss exponent which is assumed to be 0.5. The shadow fading factor ρ is a log-normal random variable with zero mean and standard deviation σ_ρ chosen as 4 dB in the simulations. The parameters for the noise models as listed in this section primarily fulfill the environment while the MS is located within the rural area. It is noticed that the reason for selecting the rural area as the simulation scenario is due to its higher probability to suffer from deficiency of signal sources. Moreover, the sampling time Δt is chosen as 1 sec in the simulations.

6.2 Validation of GPLT Scheme

6.2.1 Validation with Angle Effect

As mentioned in Section 5.1.1, the primary objective of the proposed GPLT algorithm is to adjust the position of the virtual BS such that the predicted MS can be situated at a location with minimal GDOP value. The design concept implicitly indicates that the estimation error can be reduced if the MS is possessed with a smaller GDOP value formed by its geometric layout. In this section, the relationship between the estimation errors and the GDOP values will be verified via simulations. As shown in Fig. 4, the two-BS case considered associated with the locations of the BSs are $\mathrm{BS}_1 = (505, 2{,}957)$ and $\mathrm{BS}_2 = (1{,}520, 1{,}234)$ in meters. The MS's true position is located at $\boldsymbol{x} = (1{,}020, 2{,}100)$ m. The position of the virtual BS is assumed at $\boldsymbol{x}_{v_1}(\theta) = (1{,}020 + 1{,}500\cos\theta,\ 2{,}100 + 1{,}500\sin\theta)$ m with $\theta = 0 \sim 359$ degree. It can be seen that the potential positions of the virtual BS are considered to be located at a distance 1,500 meters away from the MS's true position along with different relative angles θ.

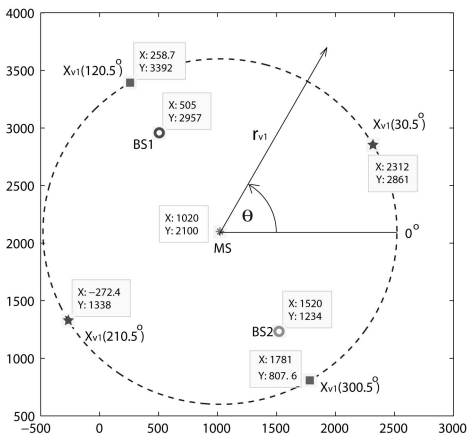

Fig. 4. An exemplify diagram for the scenarios with the two-BSs layout. Stars ($\boldsymbol{x}_{v_1}(30.5$ degree) and $\boldsymbol{x}_{v_1}(210.5$ degree)): the positions of the virtual BS cause the minimal GDOP value of the MS; Squares ($\boldsymbol{x}_{v_1}(120.5$ degree) and $\boldsymbol{x}_{v_1}(300.5$ degree)): the positions of the virtual BS cause the maximal GDOP value of the MS.

Fig. 5 illustrates the comparison between the average position error (as in Fig. 5a), the root-mean-square error (RMSE, as in Fig. 5b), and the GDOP value versus the relative angle (θ) between the true MS and the virtual BS. It is noted that the average position error (Δx) and the RMSE are computed as: $\Delta x = [\sum_{i=1}^{N} \|\boldsymbol{x} - \hat{\boldsymbol{x}}(i)\|]/N$ and $\mathrm{RMSE} = [\sum_{i=1}^{N} \|\boldsymbol{x} - \hat{\boldsymbol{x}}(i)\|^2/N]^{1/2}$, where $N = 50$ indicates the number of simulation runs. It is also noticed that the GDOP value ($\mathrm{G}_{\boldsymbol{x}}$) is evaluated at the MS's true position; while the estimated MS's position $\hat{\boldsymbol{x}}(i)$ is obtained by the two-step LS estimator employing the various positions of the virtual BS, i.e., $\boldsymbol{x}_{v_1}(\theta)$ for $\theta = 0 \sim 359$ degree. It can be observed from both plots in Fig. 5 that the average position error and the RMSE follow the similar trend as the computed GDOP value. Both the minimal average estimation error (associated with the RMSE) and the minimal GDOP value occur at the locations of $\boldsymbol{x}_{v_1}(30.5\ \text{degree}) = (2{,}312, 2{,}861)\ \text{m}$ and $\boldsymbol{x}_{v_1}(210.5\ \text{degree}) = (-272.4, 1{,}338)\ \text{m}$. It is noted that the angle θ_k^m for the minimal GDOP value can also be directly computed and verified from (24). Moreover, the maximal GDOP values and the maximal estimation errors (including both the average estimation error and the RMSE) happen around the locations of $\boldsymbol{x}_{v_1}(120.5\ \text{degree}) = (258.7, 3{,}392)\ \text{m}$ and $\boldsymbol{x}_{v_1}(300.5\ \text{degree}) = (1{,}781, 807.6)\ \text{m}$. The results can

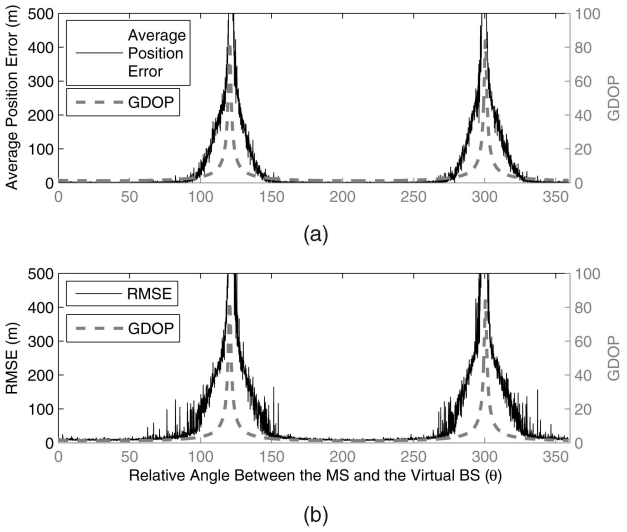

Fig. 5. (a) The average position error (solid line) and the GDOP value (dashed line) versus the relative angle between the MS and the virtual BS (θ); (b) the RMSE (solid line) and the GDOP value (dashed line) versus the relative angle between the MS and the virtual BS (θ).

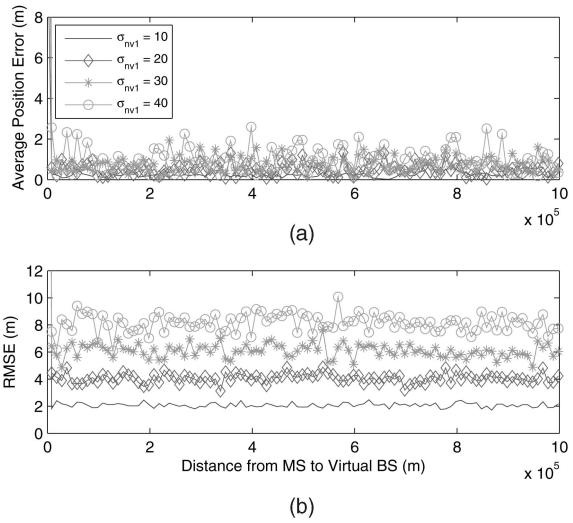

Fig. 6. (a) The average position errors versus the relative distance between the MS and the virtual BS (r_{v_1}); (b) the RMSE versus the relative distance between the MS and the virtual BS (r_{v_1}) (with $\sigma_{n_{v_1}} = 10, 20, 30, 40$).

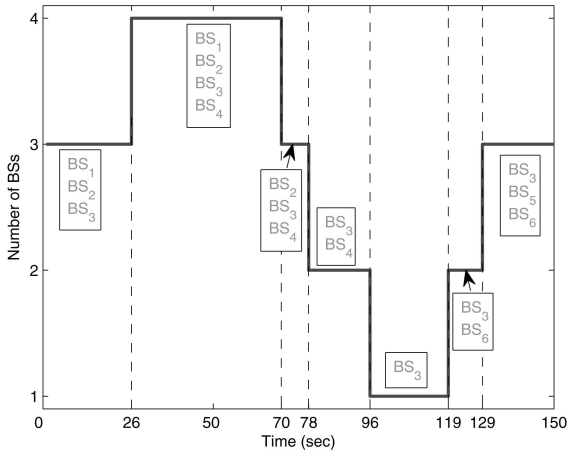

Fig. 7. Total number of available BSs (N_k) versus simulation time (second); Black textbox: available BSs ($P_{BS,k}$) during each time interval.

further be validated by observing the geometric layout, as in Fig. 4. The minimal GDOP values of the true MS occur as the three BSs form an equilateral triangle; while the maximal GDOP values happen as the three BSs are situated along a straight line. The above observations validate the effectiveness of the proposed GPLT scheme by obtaining a position of the virtual BS with a smaller GDOP value, which, consequently, reduces the corresponding estimation error. On the other hand, the estimation errors can be severely augmented if the MS happens to be located at a position with the maximum GDOP value by adopting other schemes. It can, therefore, be concluded that the results obtained from the simulations comply with the design objectives of the GPLT algorithm.

6.2.2 Validation with Distance Effect

In this section, the results obtained from Lemma 2 will be validated via simulations. It is stated in Lemma 2 that the expected value of the estimation error is independent of the distance between the MS and a specific BS (which is associated with the measurement input contaminating zero-mean random noises) by adopting the WLS location estimation algorithm. In order to validate Lemma 2 by the simulation data, the estimation errors induced by adopting the two-step LS estimator will be obtained for the evaluation of the distance effect. Fig. 6 illustrates the average position error (as in Fig. 6a) and the RMSE (as in Fig. 6b) acquired from the two-step LS method under different relative distances between the MS and the virtual BS (i.e., r_{v_1}). It is noted that the distance r_{v_1} is simulated from 1 to 10^6 m along the angle $\theta = 60$ degree, as shown in Fig. 4. The four simulated results are conducted under different signal standard deviations (i.e., $\sigma_{n_{v_1}} = 10, 20, 30, 40$) in order to examine the potential effect from the signal variances. As can be expected, the estimation errors are observed to be independent of the relative distance between the MS and the virtual BS, which are similar to the results as concluded from Lemma 2. Moreover, it is also reasonable to perceive that the increases on the signal standard deviation $\sigma_{n_{v_1}}$ will induce proportional augmentation on the RMSE (in Fig. 6b); while the average position error is considered not related to the changes due to the signal variations (in Fig. 6a). From the above observations via the simulation data, the uncorrelated relationship between the distance r_{v_1} and the estimation error is found to be consistent with the results as acquired from Lemma 2. However, a feasible value of r_{v_1} should be selected in the simulations in order not to exceed the limitation of computation, e.g., matrix inversion can result in singular value as an extremely large value of r_{v_1} is exploited. For fair comparison purpose, the distance r_{v_1} for the GPLT scheme is chosen to be the same as that in the PLT scheme in the following section.

6.3 Simulation Results

The performance comparisons between the EKF scheme, KT scheme, the CLT scheme, and the proposed PLT and GPLT algorithms are conducted under the rural environment. Fig. 7 illustrates the scenario with various numbers of BSs

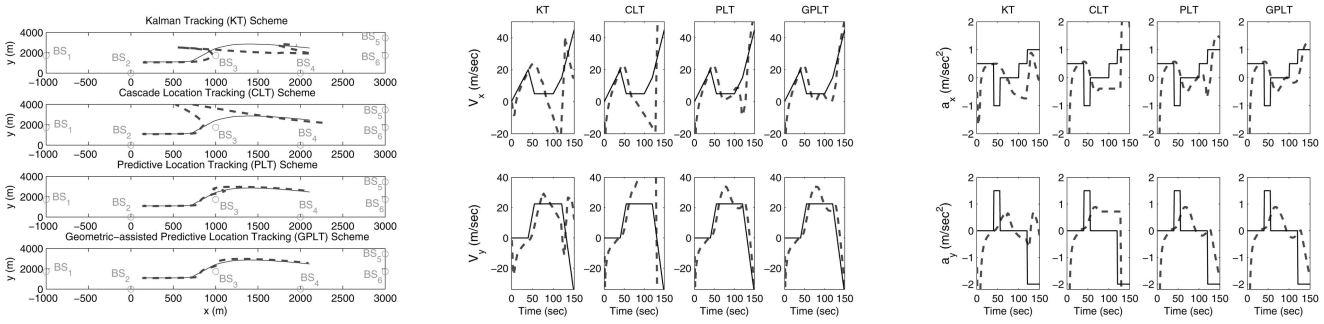

Fig. 8. Performance comparison of MS tracking. (Dashed lines: estimated value; Solid lines: true value; Empty circles in (a): the position of the BSs). (a) Trajectory. (b) Velocity. (c) Acceleration.

(i.e., the N_k values) that are available at different time intervals, where $P_{BS,k}$ denotes the set of available BSs (as indicated in Fig. 8a) that are visible during each time interval. It can be seen that the number of BSs becomes insufficient (i.e., $N_k < 3$) from the time interval of $t = 78$ to 129 sec. The total simulation interval is set as 150 seconds.

Figs. 8a, 8b, and 8c illustrate the performance comparisons of the trajectory, the velocity, and the acceleration tracking using the four algorithms. The estimated values obtained from these schemes are illustrated via the dashed lines; while the true values are denoted by the solid lines. The locations of the BSs are represented by the empty circles as in Fig. 8a. The acceleration is designed to vary at time $t = 40, 55, 100$, and 120 sec from $\boldsymbol{a}_k = (a_{x,k},\ a_{y,k}) = (0.5, 0), (-1, 1.5), (0, 0), (0.5, 0),$ to $(1, -2)$ m/sec^2 (as shown in Fig. 8c). It is noted that the number of BSs becomes insufficient during the second acceleration change (i.e., at $t = 78$ sec). Table 1 illustrates the performance comparison between the five location tracking algorithms under different percentages of average position errors, i.e., by sorting the estimation errors during the entire simulation interval. It can be observed that both the proposed GPLT and the PLT schemes provide better performance compared with the other existing algorithms owing to their consideration of insufficient signal sources, e.g., the GPLT algorithm outperforms the CLT scheme with around 560 m of estimation error under 80 percent of average position error. It is also noticed that the EKF scheme possesses the worst performance compared with the other algorithms under different percentages of estimation errors. Therefore, only the KT, the CLT, the PLT, and the GPLT schemes are further compared for performance evaluation.

By observing the starting time interval between $t = 0$ and 77 sec (where the number of BSs is sufficient), the four algorithms provide similar performance on location tracking, as shown in the $x - y$ plots in Fig. 8a. As illustrated in Figs. 8b and 8c, it can be seen that the KT scheme can provide better performance on the velocity and acceleration tracking during the transient phase (i.e, from $t = 0$ to 10 sec) compared with the other schemes. The reason can be attributed to the inherent architecture difference, as shown in Fig. 1. The KT scheme is designed to be a unified scheme which compromises between the estimated state variables, $\hat{\boldsymbol{x}}_k$, $\hat{\boldsymbol{v}}_k$, and $\hat{\boldsymbol{a}}_k$. On the other hand, the CLT algorithm associated with the PLT/GPLT schemes are designed to be a cascaded structure, where the measurement input of the Kalman filter is the resulting estimated MS's position from the two-step LS method. The estimated position of the MS dominates the update of the state variables; while both the velocity and the acceleration are considered less essential compared with the update of the position $\hat{\boldsymbol{x}}_k$. Consequently, comparable better velocity and acceleration updates are observed by adopting the KT scheme during the transient response, as in Figs. 8b and 8c. However, the KT scheme results in the worst performance among the four schemes after the transient phase (as shown in Figs. 8b and 8c). Owing to the utilization of an external location estimator within the KT scheme, the estimation errors are increasingly accumulated due to the potential inaccuracy of the estimator.

During the time interval between $t = 78$ and 129 sec with inadequate signal sources, it can be observed that only the proposed GPLT scheme can achieve satisfactory performance in the trajectory, the velocity, and the acceleration tracking. The estimated trajectories obtained from both the KT and the CLT schemes diverge from the true trajectories due to the inadequate number of measurement inputs. It is noticed that the inaccuracy within the PLT scheme primarily results from the implicitly worse geometric layout

TABLE 1
Performance Comparison between the Location Tracking Algorithms (Average Position Error (m))

	10%	20%	30%	40%	50%	60%	70%	80%	90%	100%
EKF	33.83	37.65	42.60	417.11	968.97	1430.33	2029.04	2698.13	3161.70	3344.07
KT	37.33	46.86	50.70	67.85	110.01	139.53	246.45	474.13	926.54	2026.95
CLT	19.34	26.05	27.21	46.53	72.86	198.88	327.65	671.46	1184.14	1949.06
PLT	19.34	26.05	27.21	48.58	63.07	70.90	86.13	117.44	188.14	268.89
GPLT	19.34	26.05	27.21	48.58	64.12	77.51	99.50	113.70	143.69	196.51

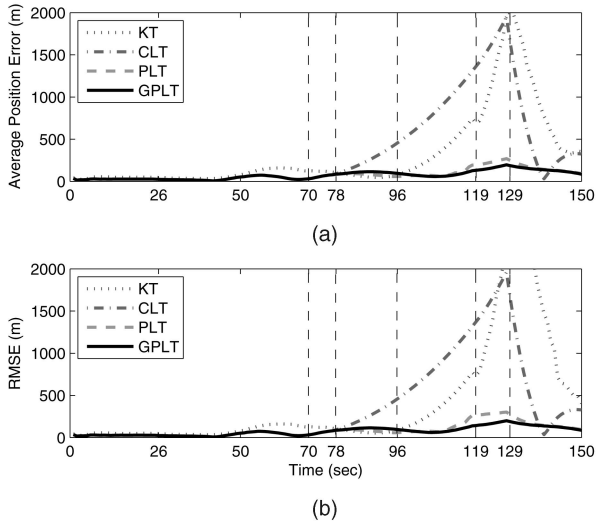

Fig. 9. (a) The average position error versus the simulation time (second); (b) the RMSE versus the simulation time (second).

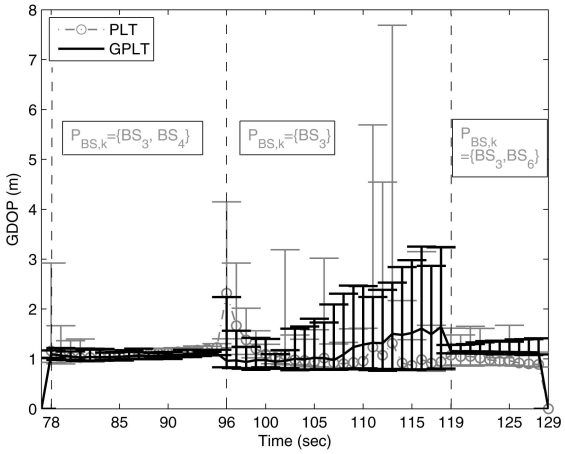

Fig. 10. Comparison of the average GDOP values (associated with their confident intervals) between the PLT and the GPLT schemes during the time interval with deficient signal sources.

at certain time instants, which will further be explained by the GDOP plot, as in Fig. 10.

Moreover, Fig. 9 illustrate the average position error (as in Fig. 9a) and the RMSE (as in Fig. 9b) (i.e., characterizing the signal variances) for location estimation and tracking of the MS. The four location tracking schemes are compared based on the same simulation scenario as shown in Fig. 7. It can be observed from both plots that the proposed GPLT and PLT algorithms outperform the conventional KT and CLT schemes. The main differences between these algorithms occur while the signal sources become insufficient within the time interval between $t = 78$ and 129 sec. The proposed GPLT and PLT schemes can still provide consistent location estimation and tracking; while the other two algorithms result in significantly augmented estimation errors. The major reason is attributed to the assisted information that is fed back into the location estimator while the signal sources are deficient. Furthermore, the GPLT algorithm outperforms the PLT scheme primarily due to its exploitation of the GDOP criterion.

The comparison of the average GDOP values (associated with their confident intervals) between the PLT and the GPLT schemes is illustrated in Fig. 10. It is noted that the averaged GDOP values are computed based on 25 simulation runs. The average GDOP values are compared only during the time interval with deficient signal sources, i.e., while the virtual BSs and the virtual measurements are exploited in both schemes. It can be observed that the GDOP values obtained from the GPLT algorithm are consistent during the simulation period with reasonable variations. On the other hand, the GDOP values acquired from the PLT scheme result in larger variations, especially during the time interval of $t = 96$-119 sec. The results are consistent with those estimation errors as acquired from Fig. 9 that worse GDOP value will result in incorrect location estimation of the MS. During the time interval of $t = 78$-95 sec, the GDOP values obtained from both schemes are considered similar, which represent that comparable geometric topology are formed by their individual virtual BSs. The geometric effect will not be an influential factor as regards the estimation error for the MS. On the other hand, during the time interval of $t = 110$-119, sudden deviates in the GDOP values are observed by using the PLT scheme. The larger average position error and the RMSE within the PLT algorithm (as seen from Fig. 9 at around $t = 120$ sec) can, therefore, be attributed to the corresponding increased GDOP values and variations. Nevertheless, with the adoption of the minimal GDOP criterion, the proposed GPLT scheme can still maintain consistent GDOP values under different numbers of available signal inputs. The resulting estimation error and RMSE can, consequently, be controlled within a reliable interval.

7 Conclusion

In this paper, the PLT and the GPLT schemes are proposed. The predictive information obtained from the Kalman filtering formulation is exploited as the additional measurement inputs for the location estimator. With the feedback information, sufficient signal sources become available for location estimation and tracking of a mobile device. Moreover, the GPLT algorithm adjusts the locations of its virtual Base Stations based on the GDOP criterion. It is shown in the simulation results that the proposed GPLT algorithm can provide consistent accuracy for location estimation and tracking even under the environments with insufficient signal sources.

Appendix

The proof of Lemma 2 in Section 5.1.2 is shown below.

Proof. Considering three TOA measurements are available for estimating the MS's position (as described in (1) with $N_k = 3$), it is assumed that the third TOA measurement $r_{3,k}$ is only contaminated by random noises with zero-mean value, i.e., $E[n_{3,k}] = 0$ and $e_{3,k} = 0$ in (1). The target of this proof is to illustrate that the expected value of the estimation error resulting from the WLS method is independent of the magnitude of the measurement input $r_{3,k}$. By combining (1) and (2), the following matrix format can be obtained:

$$\mathbf{A}_k \boldsymbol{b}_k = \mathbf{J}_k, \tag{29}$$

where

$$\boldsymbol{b}_k = [x_k \quad y_k \quad \beta_k]^T,$$

$$\mathbf{A}_k = \begin{bmatrix} -2x_{1,k} & -2y_{1,k} & 1 \\ -2x_{2,k} & -2y_{2,k} & 1 \\ -2x_{3,k} & -2y_{3,k} & 1 \end{bmatrix}, \qquad \mathbf{J}_k = \begin{bmatrix} r_{1,k}^2 - \kappa_{1,k} \\ r_{2,k}^2 - \kappa_{2,k} \\ r_{3,k}^2 - \kappa_{3,k} \end{bmatrix}.$$

It is noted that $\beta_k = x_k^2 + y_k^2$ and $\kappa_{i,k} = x_{i,k}^2 + y_{i,k}^2$, for $i = 1$, 2, and 3. Based on (29), the MS's estimated position by adopting the WLS method (i.e., $\hat{\boldsymbol{x}}_k = [\hat{x}_k,\ \hat{y}_k]^T$) can be acquired as

$$\hat{\boldsymbol{x}}_k = \mathbf{C}\left(\mathbf{A}_k^T \boldsymbol{\Psi}^{-1} \mathbf{A}_k\right)^{-1} \mathbf{A}_k^T \boldsymbol{\Psi}^{-1} \mathbf{J}_k, \tag{30}$$

where

$$\mathbf{C} = \begin{bmatrix} 1 & 0 & 0 \\ 0 & 1 & 0 \end{bmatrix}, \tag{31}$$

$$\boldsymbol{\Psi} = E[\psi\psi^T] = E[(\mathbf{J}_k - \mathbf{A}_k\boldsymbol{b}_k)(\mathbf{J}_k - \mathbf{A}_k\boldsymbol{b}_k)^T] = 4c^2\mathbf{BLB}. \tag{32}$$

The parameter $\boldsymbol{\Psi}$ is denoted as the error covariance matrix, where $\mathbf{B} = \mathrm{diag}\{\zeta_{1,k},\ \zeta_{2,k},\ \zeta_{3,k}\}$. $\mathbf{L}$ represents the covariance matrix of measured noise. The primary concern of this proof is to acquire the expected value of the estimation error $\Delta\hat{\boldsymbol{x}}_k = [\Delta\hat{x}_k,\ \Delta\hat{y}_k]^T$, which can be obtained by rewriting (30) as

$$\Delta\hat{\boldsymbol{x}}_k = \mathbf{C}\left(\mathbf{A}_k^T \boldsymbol{\Psi}^{-1} \mathbf{A}_k\right)^{-1} \mathbf{A}_k^T \boldsymbol{\Psi}^{-1} \Delta\mathbf{J}_k. \tag{33}$$

It is noted that (33) indicates that the estimation error vector $\Delta\hat{\boldsymbol{x}}_k$ is incurred by the variation within the vector $\mathbf{J}_k$. The value of $\Delta\mathbf{J}_k$ is obtained by considering the variations from the measurement inputs as (i.e., $r_{i,k} = \zeta_{i,k} + n_{i,k} + e_{i,k}$ in (1))

$$\begin{aligned} \Delta\mathbf{J}_k &= \begin{bmatrix} 2\zeta_{1,k}\ (n_{1,k} + e_{1,k}) + (n_{1,k} + e_{1,k})^2 \\ 2\zeta_{2,k}\ (n_{2,k} + e_{2,k}) + (n_{2,k} + e_{2,k})^2 \\ 2\zeta_{3,k}\ n_{3,k} + n_{3,k}^2 \end{bmatrix} \\ &\simeq \begin{bmatrix} 2\zeta_{1,k}\ (n_{1,k} + e_{1,k}) \\ 2\zeta_{2,k}\ (n_{2,k} + e_{2,k}) \\ 2\zeta_{3,k}\ n_{3,k} \end{bmatrix}, \end{aligned} \tag{34}$$

where $e_{3,k}$ equals to zero as mentioned at the beginning of this proof. It is noted that the approximation from the second equality within (34) is valid by considering that the noiseless distance $\zeta_{i,k}$ is, in general, larger than the combined noise effect $(n_{i,k} + e_{i,k})$. For simplicity and without loss of generality, a coordinate transformation can be adopted within (33) such that $(x_{1,k},\ y_{1,k}) = (0, 0)$. It is also noted that $E[n_{3,k}] = 0$. Therefore, the expected value of the estimation error (i.e., $\Delta\hat{\boldsymbol{x}}_k = [\Delta\hat{x}_k,\ \Delta\hat{y}_k]^T$) can, therefore, be acquired by expanding (33) as

$$\begin{aligned} E[\Delta\hat{x}_k] = E\{&[\zeta_{1,k}(y_{2,k} - y_{3,k})(n_{1,k} + e_{1,k}) \\ &+ \zeta_{2,k}y_{3,k}(n_{2,k} + e_{2,k})]/[x_{3,k}y_{2,k} - x_{2,k}y_{3,k}]\}, \end{aligned} \tag{35}$$

$$\begin{aligned} E[\Delta\hat{y}_k] = E\{&[\zeta_{1,k}(x_{2,k} - x_{3,k})(n_{1,k} + e_{1,k}) \\ &+ \zeta_{2,k}x_{3,k}(n_{2,k} + e_{2,k})]/[y_{3,k}x_{2,k} - y_{2,k}x_{3,k}]\}. \end{aligned} \tag{36}$$

From (35) and (36), it can clearly be observed that the expected value of the estimation error (i.e., $E[\Delta\hat{\boldsymbol{x}}_k] = [E[\Delta\hat{x}_k],\ E[\Delta\hat{y}_k]]^T$) is independent of the measured distance $r_{3,k}$ under the assumption that its associated measurement noise $n_{3,k}$ is considered a zero-mean random variable, i.e., $E[r_{3,k}] = E[\zeta_{3,k}] + E[n_{3,k}] = E[\zeta_{3,k}]$. This completes the proof. □

ACKNOWLEDGMENTS

This work was funded in part by the MOE ATU Program 95W803C, NSC 96-2221-E-009-016, the MediaTek Research Center at the National Chiao Tung University, and the Universal Scientific Industrial (USI), Taiwan.

REFERENCES

[1] F.C. Commission, *Revision of the Commissions Rules to Insure Compatibility with Enhanced 911 Emergency Calling Systems*, 1996.
[2] N. Patwari, J.N. Ash, S. Kyperountas, A.O. Hero III, R.L. Moses, and N.S. Correal, "Locating the Nodes: Cooperative Localization in Wireless Sensor Networks," *IEEE Signal Processing Magazine*, vol. 22, no. 4, pp. 54-69, July 2005.
[3] S. Gezici, Z. Tian, G.B. Giannakis, H. Kobayashi, A.F. Molisch, H.V. Poor, and Z. Sahinoglu, "Localization via Ultra-Wideband Radios: A Look at Positioning Aspects for Future Sensor Networks," *IEEE Signal Processing Magazine*, vol. 22, no. 4, pp. 70-84, July 2005.
[4] S. Hara, D. Zhao, K. Yanagihara, J. Taketsugu, K. Fukui, S. Fukunaga, and K. Kitayama, "Propagation Characteristics of IEEE 802.15.4 Radio Signal and Their Application for Location Estimation," *Proc. IEEE Vehicular Technology Conf.*, pp. 97-101, June 2005.
[5] S. Feng and C.L. Law, "Assisted GPS and Its Impact on Navigation in Intelligent Transportation Systems," *Proc. IEEE Int'l Conf. Intelligent Transportation Systems*, pp. 926-931, June 2002.
[6] P. Farradyne, *Vehicle Infrastructure Integration (VII)—Architecture and Functional Requirements*, draft, version 1.0, Apr. 2005.
[7] Y. Zhao, "Standardization of Mobile Phone Positioning for 3G Systems," *IEEE Comm. Magazine*, vol. 40, no. 7, pp. 108-116, July 2002.
[8] H. Koshima and J. Hoshen, "Personal Locator Services Emerge," *IEEE Spectrum*, vol. 37, no. 2, pp. 41-48, Feb. 2000.
[9] J.H. Reed, K.J. Krizman, B.D. Woerner, and T.S. Rappaport, "An Overview of the Challenges and Progress in Meeting the E-911 Requirement for Location Service," *IEEE Comm. Magazine*, vol. 36, no. 4, pp. 30-37, Apr. 1998.
[10] A.H. Sayed, A. Tarighat, and N. Khajehnouri, "Network-Based Wireless Location: Challenges Faced in Developing Techniques for Accurate Wireless Location Information," *IEEE Signal Processing Magazine*, vol. 22, no. 4, pp. 25-40, July 2005.
[11] W.H. Foy, "Position-Location Solutions by Taylor-Series Estimation," *IEEE Trans. Aerospace and Electronic Systems*, vol. AES-12, no. 2, pp. 187-194, Mar. 1976.
[12] X. Wang, Z. Wang, and B. O'Dea, "A TOA-Based Location Algorithm Reducing the Errors Due to Non-Line-of-Sight (NLOS) Propagation," *IEEE Trans. Vehicular Technology*, vol. 52, no. 1, pp. 112-116, Jan. 2003.
[13] Y.T. Chen and K.C. Ho, "A Simple and Efficient Estimator for Hyperbolic Location," *IEEE Trans. Signal Processing*, vol. 42, no. 8, pp. 1905-1915, Aug. 1994.
[14] L. Cong and W. Zhuang, "Hybrid TDOA/AOA Mobile User Location for Wideband CDMA Cellular Systems," *IEEE Trans. Wireless Comm.*, vol. 1, no. 3, pp. 439-447, July 2002.
[15] J. Caffery Jr., "A New Approach to the Geometry of TOA Location," *Proc. IEEE Vehicular Technology Conf.*, pp. 1943-1949, Sept. 2000.
[16] S. Venkatraman and J. Caffery Jr., "Hybrid TOA/AOA Techniques for Mobile Location in Non-Line-of-Sight Environments," *Proc. IEEE Wireless Comm. and Networking Conf.*, pp. 274-278, Mar. 2004.

[17] T. Liu, P. Bahl, and I. Chlamtac, "Mobility Modeling, Location Tracking, and Trajectory Prediction in Wireless ATM Networks," *IEEE J. Selected Areas in Comm.,* vol. 16, no. 6, pp. 922-936, Aug. 1998.
[18] Z.R. Zaidi and B.L. Mark, "Real-Time Mobility Tracking Algorithms for Cellular Networks Based on Kalman Filtering," *IEEE Trans. Mobile Computing,* vol. 4, no. 2, pp. 195-208, Mar. 2005.
[19] R.G. Brown and P.Y. Hwang, *Introduction to Random Signals and Applied Kalman Filtering,* third ed. John Wiley & Sons, 1997.
[20] J. Shuhong, S. Xicai, and K. Fanru, "A Time-of Arrival Location Algorithm for Maneuvering Target on Two-Dimensional Surface," *Proc. IEEE Int'l Conf. Signal Processing,* pp. 1700-1703, Oct. 1998.
[21] M. Nájar and J. Vidal, "Kalman Tracking Based on TDOA for UMTS Mobile Location," *Proc. IEEE Int'l Symp. Personal, Indoor and Mobile Radio Comm.,* pp. 45-49, Sept. 2001.
[22] M. Nájar and J. Vidal, "Kalman Tracking for Mobile Location in NLOS Situations," *Proc. IEEE Int'l Symp. Personal, Indoor and Mobile Radio Comm.,* pp. 2203-2207, Sept. 2003.
[23] B.L. Le, K. Ahmed, and H. Tsuji, "Mobile Location Estimator with NLOS Mitigation Using Kalman Filtering," *Proc. IEEE Conf. Wireless Comm. and Networking,* pp. 1969-1973, Mar. 2003.
[24] C.L. Chen and K.F. Feng, "Hybrid Location Estimation and Tracking System for Mobile Devices," *Proc. IEEE Vehicular Technology Conf.,* pp. 2648-2652, June 2005.
[25] N. Levanon, "Lowest GDOP in 2-D Scenarios," *IEE Proc. Radar, Sonar and Navigation,* pp. 149-155, June 2002.
[26] J. Chaffee and J. Abel, "GDOP and the Cramer-Rao Bound," *Proc. IEEE Position Location and Navigation System (PLANS) Conf.,* pp. 663-668, Apr. 1994.
[27] Y. Qi, H. Kobayashi, and H. Suda, "Analysis of Wireless Geolocation in a Non-Line-of-Sight Environment," *IEEE Trans. Wireless Comm.,* vol. 5, no. 3, pp. 672-681, Mar. 2006.
[28] Y. Qi, T. Asai, H. Yoshino, and N. Nakajima, "On Geolocation in Ill-Conditioned BS-MS Layouts," *Proc. IEEE Int'l Conf. Acoustics, Speech, and Signal Processing,* pp. 697-700, Mar. 2005.
[29] P.C. Chen, "A Cellular Based Mobile Location Tracking," *Proc. IEEE Vehicular Technology Conf.,* pp. 1979-1983, May 1999.
[30] Y.-C. Lin, P.-H. Tseng, and K.-T. Feng, "A Predictive Location Tracking Algorithm for Mobile Devices with Deficient Signal Sources," *Proc. IEEE Vehicular Technology Conf.,* pp. 859-863, Apr. 2007.
[31] L.J. Greenstein, V. Erceg, Y.S. Yeh, and M.V. Clark, "A New Path-Gain/Delay-Spread Propagation Model for Digital Cellular Channels," *IEEE Trans. Vehicular Technology,* vol. 46, no. 2, pp. 477-485, May 1997.
[32] C.Y. Lee, *IMobile Communications Engineering.* McGraw-Hill, 1993.
[33] P.C. Chen, "A Non-Line-of-Sight Error Mitigation Algorithm in Location Estimation," *Proc. IEEE Wireless Comm. Networking Conf.,* pp. 316-320, Sept. 1999.

Po-Hsuan Tseng received the BS degree in communication engineering in 2005 from the National Chiao Tung University, Hsinchu, Taiwan, where he is currently working toward the PhD degree with the Department of Communication Engineering. His current research interests include wireless location technologies and mobile WiMax system design. He is a student member of the IEEE.

Kai-Ten Feng received the BS degree from the National Taiwan University, Taipei, in 1992, the MS degree from the University of Michigan, Ann Arbor, in 1996, and the PhD degree from the University of California, Berkeley, in 2000. Between 2000 and 2003, he was with OnStar Corporation, a subsidiary of General Motors Corporation, as an in-vehicle development manager/senior technologist, working on the design of future Telematics platforms and in-vehicle networks. Between February 2003 and July 2007, he was an assistant professor with the Department of Communication Engineering, National Chiao Tung University, Hsinchu, Taiwan, where since August 2007, he has been an associate professor. His current research interests include cooperative and cognitive networks, mobile ad hoc and sensor networks, embedded system design, wireless location technologies, and Intelligent Transportation Systems (ITSs). He received the Best Paper Award from the IEEE Vehicular Technology Conference Spring 2006, which ranked his paper first among the 615 accepted papers. He is also the recipient of the Outstanding Young Electrical Engineer Award in 2007 from the Chinese Institute of Electrical Engineering (CIEE). He has served on the technical program committees of VTC, ICC, and APWCS. He is a member of the IEEE.

Yu-Chiun Lin received the BS and MS degrees in communication engineering from the National Chiao Tung University, Hsinchu, Taiwan, in 2005 and 2007, respectively. Since January 2008, he has been with Pegatron Corporation, Taipei, Taiwan, as an executive engineer. His current research interests include wireless location technologies.

Chao-Lin Chen received the BS and MS degrees in communication engineering from the National Chiao Tung University, Hsinchu, Taiwan, in 2003 and 2006, respectively. He was with the Department of Electronics Engineering, National Chiao Tung University, as a teaching assistant between August 2006 and July 2007. Since October 2007, he has been with TrendChip Technologies Corporation, Hsinchu, Taiwan, as an executive engineer. His current research interests include wireless location technologies and cooperative and cognitive networks.